

# The response of a helium white dwarf to an exploding type Ia supernova

Oded Papish<sup>1</sup>, Noam Soker<sup>1</sup>, Enrique García-Berro<sup>2,3</sup>, and Gabriela Aznar-Siguán<sup>2,3</sup>

## ABSTRACT

We conduct numerical simulations of the interacting ejecta from an exploding CO white dwarf (WD) with a He WD donor in the double-detonation scenario for Type Ia supernovae (SNe Ia), and study the possibility of exploding the companion WD. We also study the long time imprint of the collision on the supernova remnant. When the donor He WD has a low mass,  $M_{\text{WD}} = 0.2M_{\odot}$ , it is at a distance of  $\sim 0.08R_{\odot}$  from the explosion, and helium is not ignited. The low mass He WD casts an ‘ejecta shadow’ behind it. By evolving the ejecta for longer times, we find that the outer parts of the shadowed side are fainter and its boundary with the ambient gas is somewhat flat. More massive He WD donors,  $M_{\text{WD}} \simeq 0.4M_{\odot}$ , must be closer to the CO WD to transfer mass. At a distance of  $a \lesssim 0.045R_{\odot}$  helium is detonated and the He WD explodes, leading to a triple detonation scenario. In the explosion of the donor WD approximately  $0.15M_{\odot}$  of unburned helium is ejected. This might be observed as a peculiar type Ib supernova.

*Subject headings:* ISM: supernova remnants — supernovae: stars: binary — binaries: close — hydrodynamics — supernovae: general

## 1. INTRODUCTION

Type Ia Supernovae (SNe Ia) are one of the most energetic events in the universe, now known to be originated by thermonuclear detonations of carbon-oxygen (CO) white dwarfs (Hoyle & Fowler 1960). Several possible scenarios leading to a SN Ia outburst are

---

<sup>1</sup>Department of Physics, Technion – Israel Institute of Technology, Haifa 32000, Israel; papish@tx.technion.ac.il; soker@physics.technion.ac.il.

<sup>2</sup>Departament de Física Aplicada, Universitat Politècnica de Catalunya, c/Esteve Terrades 5, 08860 Castelldefels, Spain

<sup>3</sup>Institute for Space Studies of Catalonia, c/Gran Capità 2–4, Edif. Nexus 201, 08034 Barcelona, Spain

currently envisaged, although there might be some overlap between them. All scenarios have advantages and drawbacks (e.g., Tsebrenko & Soker 2015b), and there is not yet a general consensus on the leading scenario for SN Ia. In fact, it is well possible that all of them contribute to the total SN Ia rate in some unknown fraction.

These scenarios can be listed as follows, according to alphabetical order. (a) *The core-degenerate (CD) scenario* (e.g., Livio & Riess 2003; Kashi & Soker 2011; Soker 2011; Ilkov & Soker 2012, 2013; Soker et al. 2013; Tsebrenko & Soker 2015a). Within this scenario the WD merges with the hot core of a massive asymptotic giant branch (AGB) star. In this case the explosion might occur shortly or a long time after the merger. In a recent paper, Tsebrenko & Soker (2015b) argue that at least 20%, and likely many more, of all SNe Ia come from the CD scenario. (b) *The double degenerate (DD) scenario* (e.g., Webbink 1984; Iben & Tutukov 1984). This scenario is based on the merger of two WDs. However, this scenario does not specify the subsequent evolution of the merger product, namely, how long after the merger the explosion of the remnant takes place (e.g., van Kerkwijk et al. 2010). Recent papers, for example, discuss violent mergers (e.g., Lorén-Aguilar et al. 2010; Pakmor et al. 2013) as possible channels of the DD scenario, while others consider very long delays from merger to explosion, e.g., because rapid rotation keeps the structure overstable (Tornambé & Piersanti 2013). Levanon et al. (2015) argue that the delay between merger and explosion in the DD scenario should be  $\gg 10$  yr. (c) *The single degenerate (SD) scenario* (e.g., Whelan & Iben 1973; Nomoto 1982; Han & Podsiadlowski 2004). In this scenario a white dwarf (WD) accretes mass from a non-degenerate stellar companion and explodes when its mass reaches the Chandrasekhar mass limit. (d) *The double-detonation mechanism* (e.g., Woosley & Weaver 1994; Livne & Arnett 1995). Here a sub-Chandrasekhar mass WD accumulates a layer of helium-rich material coming from a helium donor on its surface. The helium layer is compressed as more material is accreted and detonates, leading to a second detonation near the center of the CO WD (see, for instance, Shen et al. 2013 and references therein, for a recent paper). (e) *The WD-WD collision scenario* (e.g., Thompson 2011; Katz & Dong 2012; Kushnir et al. 2013; Aznar-Siguán et al. 2013). In this scenario either a tertiary star brings two WDs to collide, or the dynamical interaction occurs in a dense stellar system, where such interactions are likely. In some cases, the collision results in an immediate explosion. Despite some attractive features of this scenario, it can account for at most few per cent of all SNe Ia (Hamers et al. 2013; Prodan et al. 2013; Soker et al. 2014).

Finally, it should be mentioned that very recently it has been suggested that pycnonuclear reactions could be able to drive powerful detonations in single CO white dwarfs (Chiosi et al. 2014). This scenario – the so-called *single WD scenario* – has, however, two important shortcomings. The first one is that the typical H mass fraction found in detailed evolutionary calculations of CO WD progenitors is much smaller than that needed to ignite

the core of the WD. The second drawback of this recently suggested scenario is that most SN Ia come from WDs with masses near the Chandrasekhar limit (e.g., Seitenzahl et al. 2013; Scalzo et al. 2014), while the mass at which ignition may possibly occur in the single WD scenario is  $\sim 1.2M_{\odot}$ . Hence, this scenario would also only account for a small percentage of all SN Ia.

As mentioned earlier, there is some overlap between these scenarios. For example, in the violent merger model (Lorén-Aguilar et al. 2009; Pakmor et al. 2012) it is possible that during the first stages of the merger of the two CO WDs the small helium buffer ( $\simeq 10^{-2} M_{\odot}$ ) of the original CO WDs is ignited. In this case both the DD scenario and the double detonation mechanism operate simultaneously. Also, the double detonation mechanism might operate in the CD scenario.

In this paper we study the response of a donor star that is a He WD to an exploding CO WD with mass below the Chandrasekhar limit,  $M_{\text{WD}} \simeq 1.0 - 1.1M_{\odot}$ . These parameters fit the double detonation scenario where a very low mass helium shell triggers the SN Ia explosion of a CO WD (Bildsten et al. 2007; Shen & Bildsten 2009, 2014). We will answer five questions. (1) Does the shock wave induced by the ejecta ignite helium in the WD companion by adiabatic compression or by shock heating? (2) Is carbon in the ejecta ignited as it is shocked in the outer layers of the He WD? (3) Can mixing of helium from the donor and carbon from the ejecta lead to vigorous nuclear burning? (4) How much helium is entrained by the ejecta? (5) What is the morphology of the SNR long time after the explosion as the SN ejecta sweep some ambient medium gas? To do so we will adopt two masses for the He WD companion. First we study analytically and then numerically the impact of the SN Ia ejecta of a WD of mass  $0.43M_{\odot}$  residing at  $\sim 0.02 - 0.03R_{\odot}$  from the exploding CO WD. This setting is based on the numerical simulations of Guillochon et al. (2010), Raskin et al. (2012), and Pakmor et al. (2013), for similar (but not identical) progenitors that might lead to SN Ia. In a second step, and following Bildsten et al. (2007) and Shen & Bildsten (2009) we also consider a He WD of  $0.2M_{\odot}$  at an orbital separation of  $0.08R_{\odot}$ .

There are a number of simulations studying similar processes to those studied by us, but in the SD scenario. Marietta et al. (2000) conducted 2D simulations to study the impact of a SN Ia on a hydrogen-rich non-degenerate companion. They found that several tenths of a solar mass of hydrogen are striped from the companion into a cone with a solid angle of  $65 - 115^{\circ}$  behind the companion, depending on the type of companion. Kasen (2010) was interested in the effect of the companion on the light curve shortly, up to several days, after the explosion. Pakmor et al. (2008) found the striped hydrogen mass to be much lower, and compatible with limits from observations. Pan et al. (2010) took the companion in their 2D simulations to be a non-degenerate helium star. Pan et al. (2012a) extended the study to

3D simulations and to hydrogen-rich companions. Pan et al. (2012b) were interested in the evolution of a main sequence companion after the passage of the SN shock. We reproduce the dense conical surface found to be formed behind the companion by Pan et al. (2010) and Pan et al. (2012a), but we continue to follow the interaction of this cone with the ISM. We note that none of the papers listed above continued their simulations to the stage of interaction with the ISM, as we do in the present study. Neither they included nuclear reactions in the companion as a result of the shock. Here we study the interaction of a type Ia supernova with a He WD to examine He ignition and the SNR morphology.

Our paper is organized as follows. In section 2 we discuss and quantify the properties of the material ejected from the disrupted CO WD, while in section 3 we assess analytically the possibility of an explosive ignition. In section 4 we conduct 2D axisymmetrical numerical simulations of the interaction of the ejecta with the He WD, and we examine nuclear reactions and helium entrainment. Finally, in section 5 we summarize our results and their implications to the double detonation scenario.

## 2. EJECTA PROPERTIES

To facilitate an analytical estimate we assume that the SN Ia ejecta is already in homologous expansion, and we take the profile of Dwarkadas & Chevalier (1998)

$$\rho_{\text{SN}} = A \exp(-v/v_{\text{ejecta}}) t^{-3}, \quad (1)$$

where  $v_{\text{ejecta}}$  is a constant which depends on the mass and kinetic energy of the ejecta,

$$v_{\text{ejecta}} = 2.9 \times 10^8 E_{51}^{1/2} \left( \frac{M_{\text{SN}}}{1M_{\odot}} \right)^{-1/2} \text{ cm s}^{-1}, \quad (2)$$

$E_{51}$  is the explosion energy in units of  $10^{51}$  erg, and  $A$  is a parameter given by

$$A = 3.3 \times 10^6 \left( \frac{M_{\text{SN}}}{1M_{\odot}} \right)^{5/2} E_{51}^{-3/2} \text{ g s}^3 \text{ cm}^{-3}. \quad (3)$$

The maximum velocity of the SN Ia ejecta is  $v_{\text{SNm}} \simeq 20,000 \text{ km s}^{-1}$ . We compared this analytical profile with  $M_{\text{SN}} = 1M_{\odot}$  and  $E_{51} = 1$  with models 7D and 9C from Woosley & Kasen (2011), who calculated the explosion of WD models. The maximum velocity in the analytical profile used here is  $20,000 \text{ km s}^{-1}$ . We found our model to be practically identical to their model 7D for the outer  $0.2M_{\odot}$  of the ejecta, and somewhat slower than model 9D in that mass range. For inner mass coordinates the analytical fit is slower than models 7D and 9C of Woosley & Kasen (2011). As the outer layers determine whether the companion will be

ignited, using models 7D or 9C of Woosley & Kasen (2011) will result in an easier ignition of the companion. For that, and to keep the profile simple and flexible to changes, we use the analytical profile as given above both in the analytical and the numerical calculations.

For the analytical estimates derived in section 3 we now estimate the maximum ram pressure of the ejecta on the He WD. A cold He WD of mass  $0.43 M_{\odot}$  has a radius of  $\sim 0.015 R_{\odot}$ . As it overflows its Roche lobe, with a CO WD companion of  $1 M_{\odot}$ , in a stable mass transfer the orbital separation is  $\sim 3.3$  times this distance, namely,  $a \simeq 0.05 R_{\odot}$ . However, detailed numerical calculations show that for a powerful ignition to occur the mass transfer must be unstable (Guillochon et al. 2010), and the surface of the He WD that fills the Roche lobe can be as close as  $\sim 0.02 R_{\odot}$  to the exploding CO WD (Raskin et al. 2012; Pakmor et al. 2013).

The ram pressure of the ejecta at a distance  $r_e$  from the explosion at time  $t$  after explosion is given by

$$P_{\text{ram}} = \rho(r_e)v^2 = A \exp(-r_e/v_{\text{ejecta}}t)t^{-5}r_e^2, \quad (4)$$

where  $v = r_e/t$ . The maximum ram pressure is achieved at time  $t_{\text{max}} = r_e/(5v_{\text{ejecta}}) = 1(r_e/0.02 R_{\odot})$  s, and its value is

$$P_{\text{ram}}^{\text{max}} = 5.2 \times 10^{22} E_{51} \left( \frac{r_e}{0.02 R_{\odot}} \right)^{-3} \text{ erg cm}^{-3}. \quad (5)$$

At  $t = 2t_{\text{max}}$  and  $t = 3t_{\text{max}}$  the pressure drops to a value of  $0.38P_{\text{ram}}^{\text{max}}$  and  $0.12P_{\text{ram}}^{\text{max}}$ , respectively. The first material hits the WD at time  $\sim 0.02 R_{\odot}/20,000 \text{ km s}^{-1} = 0.7 \text{ s} \simeq 0.7t_{\text{max}}$ , with a ram pressure of  $0.7P_{\text{ram}}^{\text{max}}$ . Overall, the phase in which the pressure is larger than  $\sim 0.3P_{\text{ram}}^{\text{max}}$  lasts for about two seconds at  $\sim 0.02 R_{\odot}$  from the explosion. The density of the ejecta at maximum ram pressure is

$$\rho(t_{\text{max}}) = 2.5 \times 10^4 \left( \frac{M_{\text{SN}}}{1 M_{\odot}} \right) \left( \frac{r_e}{0.02 R_{\odot}} \right)^{-3} \text{ g cm}^{-3}. \quad (6)$$

### 3. CONDITIONS FOR NUCLEAR IGNITION

Fig. 1 shows two of the physical quantities of a  $0.43 M_{\odot}$  He WD which are relevant for our study, namely the pressure and density as a function of the mass coordinate  $-\log(1 - M_r/M_{\text{WD}})$ . This specific model corresponds to a WD with central temperature  $T \simeq 10^7$  K, which results in a surface luminosity  $\log(L/L_{\odot}) \sim -2.85$ , an otherwise typical luminosity of field white dwarfs, an effective temperature  $\log T_{\text{eff}} \simeq 3.93$ , and corresponds to a

sequence which was evolved performing full evolutionary calculations that consider the main energy sources and processes of chemical abundance changes during white dwarf evolution (Althaus et al. 2009). There are three possible ways in which the He WD or the CO ejecta might be ignited:

(1) *Shock ignition of helium.* It turns out that, for the model WD used here, He is shocked and ignited in a region where both thermal and radiation pressures play a role. In this region  $\rho \sim 10^5 \text{ g cm}^{-3}$  and  $T \simeq 1.2 \times 10^9 \text{ K}$ . A good estimate of the temperature in the shocked region of the He WD can be obtained by equating the radiation pressure to the ram pressure given in equation (5):

$$T_{\text{He}} \simeq 1.2 \times 10^9 \left( \frac{r_e}{0.04 R_\odot} \right)^{-3/4} \text{ K}. \quad (7)$$

The burning time-scale of pure helium at these conditions is  $\sim 10 \text{ s}$ , just a little longer than the timescale of the dynamical flow, defined as the ejecta speed divided by the He WD radius,  $\sim 0.04 R_\odot / 10,000 \text{ km s}^{-1} \sim 3 \text{ s}$ . For these parameters, ignition conditions are reached for  $r \lesssim 0.04 R_\odot$ . This is compatible with the numerical results to be described in section 4.3, where the exact radius is found.

(2) *Carbon burning in the shocked ejecta.* The second possibility we explore is the ignition of carbon-rich material of the ejecta as it is shocked upon hitting the He WD. The post-shock pressure of the ejecta is dominated by radiation pressure. The temperature at maximum ram pressure is given by equation (7). For a distance to the explosion  $r_e = 0.02 R_\odot$  we find the temperature to be  $T_{\text{CO}} \simeq 2 \times 10^9 \text{ K}$ . For this temperature we expect that carbon will be burned. Nevertheless, we need to compare the burning time with the dynamical timescale of the flow,  $\tau_{\text{flow}} \sim 1 \text{ s}$ . For the scaling and parameters used in Sect. 2 the ejecta density at the time of maximum ram pressure and at a distance of  $0.02 R_\odot$  from the center of explosion is  $3.5 \times 10^4 \text{ g cm}^{-3}$ . If the carbon mass is half of the mass of the ejecta and the compression factor is  $\sim 4$ , then the post-shock density in the carbon-rich region is  $\rho_C \simeq 7 \times 10^4 \text{ g cm}^{-3} \sim 10^5 \text{ g cm}^{-3}$ . As in this scenario the companion star is much closer to the center of the explosion than the corresponding one of the single-degenerate scenario, the density of the shocked ejecta will be much higher, and the burning timescale much shorter. We find that the carbon burning timescale for this density and a typical temperature  $\sim 2 \times 10^9 \text{ K}$  to be about one second. These temperatures and densities are achieved near the stagnation point in a small region of size  $\sim 0.1 r_e$  – see below. The outflow time from this region is  $\sim 0.002 R_\odot / 1.5 \times 10^4 \text{ km s}^{-1} = 0.1 \text{ s}$ . Thus, the outflow time is shorter than the burning time scale. In the numerical results to be described next we obtain no significant carbon burning, showing that the outflow time of carbon from the shocked region is indeed very short. This is unlike the case in which helium belonging to the He WD

is shocked inside the He WD and cannot flow outward.

(3) *Igniting helium by mixing ejecta.* Even if carbon is not ignited, mixing of the ejecta at  $T \sim 10^9$  K with helium might, in principle, even if helium was not ignited by the shock, power a thermonuclear runaway. In our numerical simulations mixing is not sufficiently deep to cause ignition by this process (see section 4).

For the case of a low-mass He WD we repeated all these calculations and we found that none of the previously described processes drive a powerful nuclear outburst, and thus the evolution in this case should mostly consist of a purely hydrodynamical flow. As it will be explained in detail in the next section, full hydrodynamical numerical simulations confirm this.

## 4. NUMERICAL SIMULATIONS

### 4.1. Numerical setup

We use version 4.2.2 of the FLASH gas-dynamical numerical code (Fryxell et al. 2000). The FLASH code has been used before for a similar study in the SD scenario, in 2D (Kasen 2010; Pan et al. 2010) and 3D (Pan et al. 2012a,b). The widely used FLASH code is a publicly available code for supersonic flow suitable for astrophysical applications. The simulations are done using the unsplit PPM solver of FLASH. We use 2D axisymmetric cylindrical coordinates with an adaptive mesh refinement (AMR) grid. The origin of the grid, (0, 0), is taken at the center of the explosion. In all the figures shown below the symmetry axis of the grid is the vertical axis. The axisymmetric grid forces us to neglect the orbital relative velocity of the He WD and the exploding CO WD. In any case, the orbital velocity is much smaller than the ejecta velocity, and will have virtually no effect on our conclusions. For the equation of state we use the Helmholtz EOS (Timmes & Swesty 2000). This EOS includes contributions from partial degenerate electrons and positrons, radiation, and non-degenerate ions. We use the Aprox19 nuclear network of 19 isotopes (Timmes 1999) in FLASH. The hydrodynamic module is coupled to the nuclear network by setting the parameter `enucDtFactor=0.1` in FLASH (Hawley et al. 2012), and shock burning is disabled by default. Self gravity is included using the new multipole solver in FLASH with order  $l = 10$ .

We run our collision simulations with two different resolutions as a test for convergence and found no appreciable difference. In addition, we run a low resolution simulation on a much larger grid to follow the long time evolution of the ejecta. For the high-resolution simulations the minimum cell size was  $\sim 12 \times 12$  km with a total of 10 levels of AMR refinement. For the low-resolution simulations the minimum cell size was  $\sim 48 \times 48$  km. In

addition we lowered the resolution in the large grid simulation to  $\sim 92 \times 92$  km from initially  $\sim 46 \times 46$  km after  $t = 16$  s from the explosion to reduce the computational time.

The initial He WD mass, radius, and distance from the center of the explosion in the two simulated cases to be presented below are  $(M_{\text{WD}}, R_{\text{WD}}, a_0) = (0.2M_{\odot}, 0.02R_{\odot}, 0.082R_{\odot})$  and  $(M_{\text{WD}}, R_{\text{WD}}, a_0) = (0.43M_{\odot}, 0.015R_{\odot}, 0.029 - 0.043R_{\odot})$  for the low- and high-mass He WDs, respectively. The WDs are cold, and the radius of the  $0.43M_{\odot}$  WD is somewhat smaller than the hotter WD presented in Fig. 1. These models were built with version 6022 of the Modules for Experiments in Stellar Astrophysics (MESA; Paxton et al. 2011).

Initially, the ejecta in our simulations is homologous expanding according to equations (1)-(3), with  $E_{51} = 1$  and  $M_{\text{SN}} = 1M_{\odot}$ . The maximum velocity at the front of the ejecta is set to  $20,000 \text{ km s}^{-1}$ . Its outer radius from the center of explosion is set to almost touch the He WD. Ideally one should start from a real explosion of the CO WD. But we limit ourselves in the present study to explore the basic processes. We estimate the internal energy as follows. At shock breakout, about half the energy is thermal, half is kinetic. As the gas expands, thermal energy drops as  $1/r$ . By the time it hits the He WD the thermal energy is one third of its initial value. Most of it went to accelerate the gas to almost the terminal velocity. The kinetic energy is now  $5/6$  of the initial energy, and the thermal energy is  $1/6$ . Over all, the kinetic energy is 5 times or more higher than the thermal energy. In the simulations we therefore set the thermal energy to be 0.2 of kinetic energy at  $t = 0$  from the start of the simulations. We also simulated cases where the initial temperature was set to a very low value, and found no significant differences from the results presented here (see version V1 of this paper on astro-ph). In the figures described below time is measured from the moment at which the CO explodes. We ran our simulations with two different chemical compositions. In a first set of simulations we assumed that the ejecta was entirely made of nickel, while in a second set we adopted C/O. We found that our results are not sensitive to the adopted composition. (see version V1 of this paper on astro-ph for figures with C/O composition). Finally, we mention that radiative cooling and photon diffusion are not important for the problem simulated here, and hence have not been included in our calculations.

## 4.2. A low-mass helium WD

In the case in which a low-mass He-WD is considered, nuclear reactions are not significant and three distinct stages of the interaction can be differentiated. (i) The early interaction phase, when temperatures of the shocked gas are at maximum, and the ejecta flows around the He WD. (ii) The intermediate phase, when the shock breaks out from the



back of the WD and ejects helium from it. (iii) The late time phase, when expansion is homologous until the ejecta sweep a non-negligible ambient mass and adopts the shape of an old SNR. We ran the simulations using both the low- and high-resolutions grids. This was done for checking numerical convergence. As mentioned earlier, the low-resolution grid was designed to cover a larger region around the interacting WDs, and thus was used to follow the evolution of the SNR at late times. In the overlapping regions, the results of the two simulations with different resolutions were found to be the same.

*The early stage.* In Fig. 2 we present the density and velocity maps at several times from  $t = 2$  s (2 seconds after explosion) to the time instant at which the shock that runs through the He WD reaches the backside of the He WD ( $t = 16$  s). The SN ejecta hits the WD and flows around it, forming a dense surface with a 3D conical shape. Such dense conical surfaces appear in the 2D simulations of Pan et al. (2010) and of Pan et al. (2012a) where non-degenerate companion stars were used. In our 2D grid the dense shell has a shape of two dense stripes on the meridional plane, one at each side of the symmetry axis. Note that as mentioned in section 3 the temperatures and densities are too low to drive any significant nuclear burning.

*The intermediate stage.* In Fig. 3 we show the flow after the break-out of the shock from the back side (down flow) of the He WD, and the consequential helium outflow. Most of the ejected helium falls back to the WD as can be seen in the last panel. Only  $0.003M_{\odot}$  of helium escapes and flows outward near the symmetry axis, too small to be observed with current observational means. The strong concentration at the axis is a numerical effect. The volume inside the dense conical shell is a region of low density ejecta. The dense conical surface continues to expand and more or less preserves its shape in homologous expansion. The homologous expansion continues until the interaction with the ambient gas – the interstellar medium (ISM) or a circumstellar matter (CSM) – starts to shape the outskirts of the ejecta.

*The late stage.* We are interested in the morphology of the ejecta at hundreds of years after explosion. For numerical reasons, we let the ejecta interact with an ambient medium close to the explosion site. As the ejecta expansion is already homologous with high Mach numbers ( $\gtrsim 10$ ) at the end of the intermediate stage, the morphology obtained here at the late stage and on a scale of several solar radii represents quite well the expected morphology hundreds of year later and with a much larger size (a few pc). For the scaled numerical study of the ejecta-ambient gas interaction we set the ambient density to be  $0.01 \text{ g cm}^{-3}$ , and follow the expansion until  $t = 492$  s, when the medium mass intercepted by the ejecta is  $\sim 1M_{\odot}$ . The interaction of the dense conical surface with the ambient gas forms a circle of high pressure, with its center on the symmetry axis (half of this circle is into, and half

out of, the page). This high pressure circle accelerates gas, both ambient and ejecta, toward the relatively empty cone (toward the symmetry axis). This gas and the helium along the symmetry axis, determine the flow structure within the cone.

The morphological changes due to this flow depend on the swept ISM mass in front of the dense conical surface,  $M_s$ . The dissipated energy when the swept ISM mass is lower than the ejecta mass that interacts with it  $M_s < M_e$ , is approximately  $E_d \simeq 0.5M_s v^2$ , where  $v$  is the radial speed of the ejecta. If a fraction  $\eta$  of this energy goes into azimuthal (tangential) motion, then the azimuthal speed  $v_\theta$  is given by  $0.5M_e v_\theta^2 \simeq \eta E_d$ , from which we find  $v_\theta \sim \eta(M_s/M_e)^{1/2} v^{1/2}$ . This is a crude expression, which nonetheless shows that the filling of the empty cone depends mainly on the total swept ISM mass, and not on the ISM density which is higher in our simulation due to numerical limitations.

To form a synthetic map (in radio, X-ray synchrotron, or thermal X-ray), we integrate over density squared along the lines of sight, but considering only shocked, hot gas,

$$I(x, y) \equiv \int [\rho(x, y, z)]^2 dz, \quad (8)$$

where  $x, y$  are the coordinates on the plane of the sky and  $z$  is taken along line of sight. The interaction regions are where synchrotron emission will be formed. Although here the plots are given shortly after explosion, in this paper we mimic the structure hundreds of years after explosion, when radioactive decay is very small and does not play a role in forming the hot regions.

The obtained ‘intensity maps’ are presented in Fig. 5. Two inclinations are presented, the symmetry axis is in the plane of the sky (left), or at  $30^\circ$  to the plane of the sky (right). These are presented at two times when the swept-up ambient masses are  $\sim 0.1M_\odot$  ( $t = 202$  s upper panels), and  $\sim 1M_\odot$  ( $t = 492$  s lower panels). In Fig. 6 we present the integral of the density but only for the ejected mass,

$$N_{\text{eject}}(x, y) \equiv \int [\rho(x, y, z)_{\text{eject}}] dz \quad (9)$$

The prominent features of the SNR when the symmetry axis is close to the plane of the sky before the swept ISM gas is too large are the following ones. (a) A ‘flat front’ of the conical region (upper part in the figure which is the initial direction of the He WD); (b) A region of lower intensity at that flat front relative to the rest of the SNR front; (c) A dense conical surface in the interior; (d) The inner volume of the conical surface is almost completely devoid of ejecta gas. The first two features fade as more ambient gas (ISM) is swept. Let us note that the main result here does not depend much on whether the He WD

is younger and hotter, hence has a larger radius. It will simply have somewhat larger orbital separation. But as the double-detonation model requires stable Roche lobe overflow (RLOF), the solid angle covered by the He WD will be about the same, and so is the conical shape formed behind it (see Marietta et al. 2000). Here we find the angular size (from symmetry axis to conical surface) of the cone to be  $\sim 35^\circ$ . Marietta et al. (2000) found in their study of the single-degenerate scenario that the companion creates a ‘hole’ in the supernova debris with an angular size of  $\sim 30 - 40^\circ$ , depending on the part of the ejecta, and Pakmor et al. (2008) found an angular size of  $\sim 23^\circ$ . Most similar to our structure of the cone are the results of Pan et al. (2010), where the angular size of the cone is  $\sim 40^\circ$ , and of Pan et al. (2012a) where in many cases the angular size of the cone is  $\sim 40^\circ$  (in some 3D simulations there is no well defined cone). All these results agree with each other within the range of different initial parameters.

Although some SNRs show some dipole deviations from sphericity, we are not aware of any SNR that shows such a conical imprint morphology. One might think of SN1006, but examining the prominent features we find that SN1006 cannot be explained by such an interaction. (a) SNR SN1006 has a flat front. However, there is a hydrogen-rich optical filament along the flat front. The flat front seems to have been formed by an asymmetrical external interaction formed by asymmetrical ISM. (b) In SN1006 the X-ray intensity of the flat front is lower than the front on the orthogonal directions, but not lower than the other side of the SNR (e.g., Winkler et al. 2014). Also, SN1006 does not show a uniform intensity along the spherical parts not including the flat front. (c) A dense conical surface in the interior is not observed in SN1006 (e.g., Winkler et al. 2014) (d) As can be seen from figure 9 of Winkler et al. (2014), the volume behind the flat front is rich in neon and oxygen, and it is not poor in ejecta. We conclude that the structure of the SNR SN1006, despite the flat front on one side, is incompatible with the morphology expected from the double-detonation scenario.

The results of asymmetrical SNR obtained here applies to all single-degenerate scenarios as well. The DD scenario also leads to asymmetrical explosion if it occurs too shortly after the merger of the two WDs. Overall, it seems that the symmetrical structures of most SNRs Ia hint that when it explodes the WD is all alone. This is compatible with the CD scenario. In cases where a circumstellar gas is present and influences the SNR morphology, e.g., in forming two opposite ‘ears’ as in the Kepler SN remnant, the CD scenario seems to do better than other scenarios as well (Tsebrenko & Soker 2015b).

In some SNRs one can identify two opposite ‘ears’ that divert the SNR from being spherical (see Tsebrenko & Soker 2015b for a list of objects). These ‘ears’ might be formed by jets in the pre-explosion evolution, as expected for some SNRs in the CD scenario

(Tsebrenko & Soker 2015b). These SNRs are not perfectly spherical, but the asymmetry is like a quadrupole, and not as a dipole as expected if a companion influence the shaping of the SNR.

A word of caution is in place here. Our conclusions hold as long as there are no processes that erase the asymmetry caused by the companion. If the initial asymmetry is large, e.g., as proposed by Maeda et al. (2010), then the morphology of SNRs discussed above implies that there is a process that erases asymmetry. For example, radioactive heating of dense regions can cause them to expand and fill empty regions. However, three points should be made regarding the homogenizing effect on the flow by radioactive heating. (1) The change in velocity and density cause a deviation from the purely homologous density profile of about 10 per cent (Pinto & Eastman 2000; Woosley et al. 2007; Noebauer et al. 2012). Such small variations will not erase the dipole asymmetry. (2) The nickel is concentrated in the center, while we are interested in the outer layers that are first to interact with the ISM. (3) The observed very low level continuum polarization at the first few weeks in SN 2012fr points to a symmetrical explosion that is inconsistent with the merger-induced explosion scenario (Maund et al. 2013). Namely, it seems that explosion is not far from spherical from the beginning.

Over all, despite the caution one must take at this stage, the assumptions and approximations made here lead to a fair representation of the SNR that result from the double detonation scenario with low mass He WD as the donor.

### 4.3. A massive helium WD

In this case we place a  $0.43M_{\odot}$  He WD at closer distances than the  $0.2M_{\odot}$  one, as described in section 4.1. We find that the helium WD is ignited when the distance of its center to the center of the CO WD is  $\lesssim 3.1 \times 10^9$  cm =  $0.045R_{\odot}$ , and that practically no burning occurs if it is placed at larger distances.

In Figs. 7 to 9 we present the evolution of density, temperature, and nickel mass fraction, of the ignited He WD at 6 different times, as indicated. The initial distance of the center of the He WD from the center of explosion is  $0.043R_{\odot}$ .

Note that this calculation shares some features in common with the evolution in the case in which a low-mass He WD is considered, but also some noticeable differences. In particular, although the evolution of the hydrodynamical flow is apparently similar, the key difference is the much larger temperatures attained during the interaction between the ejecta and the He WD. Ignition of helium occurs just before  $t = 2$  s, as can be seen in the lower panels of

Fig. 10. The ignited helium raises the temperature and a thermonuclear detonation occurs, in accordance with the theoretical estimates presented in section 3. By the last panel the explosion has ended.

It is interesting to note as well the important role of radiation pressure in this simulation, as it should be expected given the considerations explained in section 3. To corroborate this, in the upper panels of Fig. 10 we show the total pressure (top) and ratio of radiation to total pressure (bottom) at the time of helium ignition,  $t = 2$  s. It can be seen that at the ignition point the radiation pressure dominates, but thermal pressure is not negligible. Also, the total pressure in the ignition region is  $\sim 10^{22}$  erg cm $^{-3}$ , comparable to the estimate given in equation (5) if we adopt  $r_e = 0.04R_\odot$ .

Given that the temperatures attained during the interaction between the ejecta and the massive He WD are rather high, extensive nuclear processing occurs, and a substantial amount of nickel is synthesized. Nickel first appears in a region laying between the center of the He WD and the surface facing the ejecta. Note that after a few seconds most of the material of the He WD has been processed to nickel. This contradicts observations, as the SNR will be highly asymmetrical, as in the violent merger simulation presented by Pakmor et al. (2012). We find that not all helium is burned and  $\sim 0.15M_\odot$  of helium is ejected from the exploding He WD. This also contradicts some observations, e.g., Mazzali & Lucy (1998) found a limit of  $< 0.1M_\odot$  of helium in SN Ia 1994D. In a recent study Lundqvist et al. (2015) put a much stronger limit of  $\lesssim 0.01M_\odot$  of ablated mass from a helium-rich companion to SN 2011fe and to SN 2014J. We conclude that the presence of a relatively close by,  $a_0 \lesssim 0.45R_\odot$ , He WD donor to the exploding CO WD leads to an explosion that has characteristics contradicting observations of SNe Ia. Accordingly, the double-detonation scenario seems to do not apply to normal SNe Ia.

We have actually simulated here a ‘triple detonation scenario’. The three stages are: He detonation on the surface of a WD, then a CO detonation, and finally a He detonation in the He WD companion. The outcome is a total ejected mass of about the Chandrasekhar mass, although the two WDs were each much below the Chandrasekhar mass. The ejected mass and synthesized nickel are larger than those inferred for SN 2005E (Perets et al. 2010), or ‘calcium-rich gap’ transients in general (Kasliwal et al. 2012; for a recent list of transients see Perets 2014). We also expect iron group elements, which are not generally observed in SN 2005E and the other ‘calcium-rich gap’ transients (Perets et al. 2010; Kasliwal et al. 2012). One of these gap transients have hydrogen (Kasliwal et al. 2012), which is not expected in the tripe-detonation scenario. Such transients are more likely to come from helium detonation on a WD without ignition of the He WD companion (Meng & Han 2014).

The presence of helium might lead to classification of the event as a SN Ib, but with high

helium-burning products that will make it a peculiar SN Ib. Such SNe might be related to the peculiar low-luminosity SNe Ib with relatively strong Ca spectral lines (e.g., Perets et al. 2010; Foley 2015). Foley (2015), following Perets et al. (2010), suggests that the progenitor system for these SNe is a double WD system where at least one WD has a significant He abundance. We here raise the possibility that some Ca-rich peculiar Ib SNe come from the triple-detonation scenario. This speculation deserves a separate study. In any case, we expect the triple-detonation scenario to be very rare.

## 5. SUMMARY AND CONCLUSIONS

We have studied the impact of the ejecta of an exploding CO WD on the donor star in the double-detonation scenario for the formation of Type Ia supernovae (SN Ia). We have done so for two masses of the secondary He WD, namely  $0.2M_{\odot}$  and  $0.43M_{\odot}$ , assuming that the SN Ia ejecta is already in homologous expansion when it hits the surface of the secondary WD. The first part of our study was done using analytical estimates, while in the second part of our work we performed full 2-dimensional hydrodynamical calculations, employing the FLASH code. Our most relevant results can be summarized as follows.

For the case in which a massive He WD ( $0.43M_{\odot}$ ) is considered, our analytical estimates predicted that the material of the He WD would undergo a powerful thermonuclear runaway when the ejected material of the exploding CO WD interacts with outer layers of the donor WD (Sect. 3). Our analytical predictions are confirmed by our detailed hydrodynamical calculations that also give us the evolution with time of the flow, where ignition occurs, the amount of nickel formed, and the mass of helium ejected by the interaction (Figs. 7 - 10). In particular, the mass of ejected helium ( $0.15M_{\odot}$ ) would have been easily detected in observations, implying that this scenario seems to be ruled out for standard SN Ia.

For the binary system containing a low-mass He WD ( $0.2M_{\odot}$ ) no significant nuclear processing occurs, and the evolution consists of an almost pure hydrodynamical flow. The evolution can be divided in three distinct phases. During the initial phase a shock runs through the outer layers of the He WD, and the SN ejecta flows around the secondary star, forming a region with conical shape (Fig. 2). In the intermediate stage, just after the shock breaks-out from the back side of the He WD, some material from the He WD is ejected but most of it falls back at later times, while a conical dense surface continues expanding (Fig. 3). Finally, during the late stages of the evolution the SN ejecta interacts with the ambient medium, which we numerically set to a very high density to mimic interaction with the ISM hundreds of years later. During this phase the conical flow previously described forms a ring of high pressure, which accelerates material towards the low-density conical region (upper

right panel of Fig. 4).

The hydrodynamical evolution previously described has observational consequences. In an attempt to model the morphology of the resulting SNR we integrated the density squared of the hot gas for two viewing angles and two times (Fig. 5). The integrated ejecta density is shown in Fig. 6). We found that the shape of the SNR, that contains a prominent flat region in the direction of the shadow of the He WD, is at odds with known SNR morphologies.

In conclusion, our study supports previous claims that the double-detonation scenario can at best be responsible for a very small fraction of all SN Ia. Specifically, Piersanti et al. (2013) claimed that the double-detonation scenario can account for only a small fraction of all SN Ia, because the parameter space leading to explosion is small. Ruiter et al. (2014), on the other hand, argued that the double-detonation model can account for a large fraction of SN Ia. For that to be the case, most ( $> 70\%$ ) of the donors in the study of Ruiter et al. (2014) are He WD. Our results show that He WD donors lead to explosions that are in contradiction with the observed morphology of the SNRs of Type Ia SN, and that if the He WD is massive ( $\sim 0.4M_{\odot}$ ), not all helium is burned and, consequently, would be spectroscopically observed, again in contradiction with observations.

There is another severe problem with the double detonation scenario (Tsebrenko & Soker 2015b). As Ruiter et al. (2014) showed, most exploding WDs in the double-detonation scenario are of mass  $< 1.1M_{\odot}$ . This is in a strong contrast with recent claims that most SN Ia masses are peak around  $1.4M_{\odot}$  (Scalzo et al. 2014). Seitenzahl et al. (2013) also claimed that at least 50% of all SN Ia come from near Chandrasekhar mass ( $M_{\text{Ch}}$ ) WDs.

All in all, we conclude that the double-detonation scenario can lead to explosions, but their characteristics are not typical of those of SN Ia. Thus, SNe Ia must be originated by other channels, most likely the core-degenerate and the double-degenerate scenarios (Tsebrenko & Soker 2015b).

We thank an anonymous referee for many detailed comments that substantially improved, both the presentation of our results and their scientific content. This research was supported by the Asher Fund for Space Research at the Technion, and the E. and J. Bishop Research Fund at the Technion. This work was also partially supported by MCINN grant AYA2011–23102, and by the European Union FEDER funds. OP is supported by the Gutwirth Fellowship.

## REFERENCES

Althaus, L. G., Panei, J. A., Romero, A. D., et al. 2009, *A&A*, 502, 207

- Aznar-Siguán, G., García-Berro, E., Lorén-Aguilar, P., José, J., & Isern, J. 2013, *MNRAS*, 434, 2539
- Bildsten, L., Shen, K. J., Weinberg, N. N., & Nelemans, G. 2007, *ApJ*, 662, L95
- Chiosi, E., Chiosi, C., Trevisan, P., Piovan, L., & Orio, M. 2014, *arXiv:1409.1104*
- Dwarkadas, V. V., & Chevalier, R. A. 1998, *ApJ*, 497, 807
- Foley, R. J. 2015, *arXiv:1501.07607*
- Fryxell B., Olson K., Ricker P., et al., 2000, *ApJS*, 131, 273
- Guillochon, J., Dan, M., Ramirez-Ruiz, E., & Rosswog, S. 2010, *ApJ*, 709, L64
- Hamers, A. S., Pols, O. R., Claeys, J. S. W., & Nelemans, G. 2013, *MNRAS*, 430, 2262
- Han, Z., & Podsiadlowski, P. 2004, *MNRAS*, 350, 1301
- Hawley, W. P., Athanassiadou, T., & Timmes, F. X. 2012, *ApJ*, 759, 39
- Hoyle, F., & Fowler, W. A. 1960, *ApJ*, 132, 565
- Iben, I., Jr., & Tutukov, A. V. 1984, *ApJS*, 54, 335
- Ilkov, M., & Soker, N. 2012, *MNRAS*, 419, 1695
- Ilkov, M., & Soker, N. 2013, *MNRAS*, 428, 579
- Kasen, D. 2010, *ApJ*, 708, 1025
- Kashi, A., & Soker, N. 2011, *MNRAS*, 417, 1466
- Kasliwal, M. M., Kulkarni, S. R., Gal-Yam, A., et al. 2012, *ApJ*, 755, 161
- Katz, B., & Dong, S. 2012, *arXiv:1211.4584*
- Kushnir, D., Katz, B., Dong, S., Livne, E., & Fernández, R. 2013, *arXiv:1303.1180*
- Levanon, N., Soker, N., & García-Berro, E. 2014, *arXiv:1408.1375*
- Livio, M., & Riess, A. G. 2003, *ApJ*, 594, L93
- Livne, E., & Arnett, D. 1995, *ApJ*, 452, 62
- Lorén-Aguilar, P., Isern, J., & García-Berro, E. 2009, *A&A*, 500, 1193



- Lorén-Aguilar, P., Isern, J., & García-Berro, E. 2010, *MNRAS*, 406, 2749
- Lundqvist, P., Nyholm, A., Taddia, F., et al. 2015, arXiv:1502.00589
- Maeda, K., Benetti, S., Stritzinger, M., et al. 2010, *Nature*, 466, 82
- Marietta, E., Burrows, A., & Fryxell, B. 2000, *ApJS*, 128, 615
- Maund, J. R., Spyromilio, J., Höflich, P. A., et al. 2013, *MNRAS*, 433, L20
- Mazzali, P. A., & Lucy, L. B. 1998, *MNRAS*, 295, 428
- Meng, X., & Han, Z. 2014, arXiv:1410.8630
- Noebauer, U. M., Sim, S. A., Kromer, M., Röpke, F. K., & Hillebrandt, W. 2012, *MNRAS*, 425, 1430
- Nomoto, K. 1982, *ApJ*, 253, 798
- Pakmor, R., Kromer, M., Taubenberger, S., et al. 2012, *ApJ*, 747, L10
- Pakmor, R., Kromer, M., Taubenberger, S., & Springel, V. 2013, *ApJ*, 770, L8
- Pakmor, R., Röpke, F. K., Weiss, A., & Hillebrandt, W. 2008, *A&A*, 489, 943
- Pan, K.-C., Ricker, P. M., & Taam, R. E. 2010, *ApJ*, 715, 78
- Pan, K.-C., Ricker, P. M., & Taam, R. E. 2012a, *ApJ*, 750, 151
- Pan, K.-C., Ricker, P. M., & Taam, R. E. 2012b, *ApJ*, 760, 21
- Paxton, B., Bildsten, L., Dotter, A., et al. 2011, *ApJS*, 192, 3
- Perets, H. B. 2014, arXiv:1407.2254
- Perets, H. B., Gal-Yam, A., Mazzali, P. A., et al. 2010, *Nature*, 465, 322
- Piersanti, L., Tornambé, A., Yungelson, L., & Straniero, O. 2013, *IAU Symposium*, 281, 209
- Pinto, P. A., & Eastman, R. G. 2000, *ApJ*, 530, 744
- Prodan, S., Murray, N., & Thompson, T. A. 2013, arXiv:1305.2191
- Raskin, C., Scannapieco, E., Fryer, C., Rockefeller, G., & Timmes, F. X. 2012, *ApJ*, 746, 62
- Ruiter, A. J., Belczynski, K., Sim, S. A., Seitenzahl, I. R., & Kwiatkowski, D. 2014, *MNRAS*, 440, L101

- Scalzo, R. A., Ruiter, A. J., & Sim, S. A. 2014, MNRAS in press.
- Seitenzahl, I. R., Cescutti, G., Röpke, F. K., Ruiter, A. J., & Pakmor, R. 2013, A&A, 559, L5
- Shen, K. J., & Bildsten, L. 2009, ApJ, 699, 1365
- Shen, K. J., & Bildsten, L. 2014, ApJ, 785, 61
- Shen, K. J., Guillochon, J., & Foley, R. J. 2013, ApJ, 770, L35
- Soker, N. 2011, arXiv:1109.4652
- Soker, N., Kashi, A., Garcia-Berro, E., Torres, S., & Camacho, J. 2013, MNRAS, 431, 1541
- Soker, N., García-Berro, E., & Althaus, L. G. 2014, MNRAS, 437, L66
- Thompson, T. A. 2011, ApJ, 741, 82
- Timmes, F. X. 1999, ApJS, 124, 241
- Timmes, F. X., & Swesty, F. D. 2000, ApJS, 126, 501
- Tornambé, A., & Piersanti, L. 2013, MNRAS, 431, 1812
- Tsebrenko, D., & Soker, N. 2014a, arXiv:1407.6231
- Tsebrenko, D., & Soker, N. 2014b, arXiv:1409.0780
- van Kerkwijk, M. H., Chang, P., & Justham, S. 2010, ApJ, 722, L157
- Webbink, R. F. 1984, ApJ, 277, 355
- Whelan, J., & Iben, I., Jr. 1973, ApJ, 186, 1007
- Winkler, P. F., Williams, B. J., Reynolds, S. P., Petre, R., Long, K. S., Katsuda, S., Hwang, U. 2014, ApJ, 781, 65
- Woosley, S. E., & Kasen, D. 2011, ApJ, 734, 38
- Woosley, S. E., Kasen, D., Blinnikov, S., & Sorokina, E. 2007, ApJ, 662, 487
- Woosley, S. E., & Weaver, T. A. 1994, ApJ, 423, 371

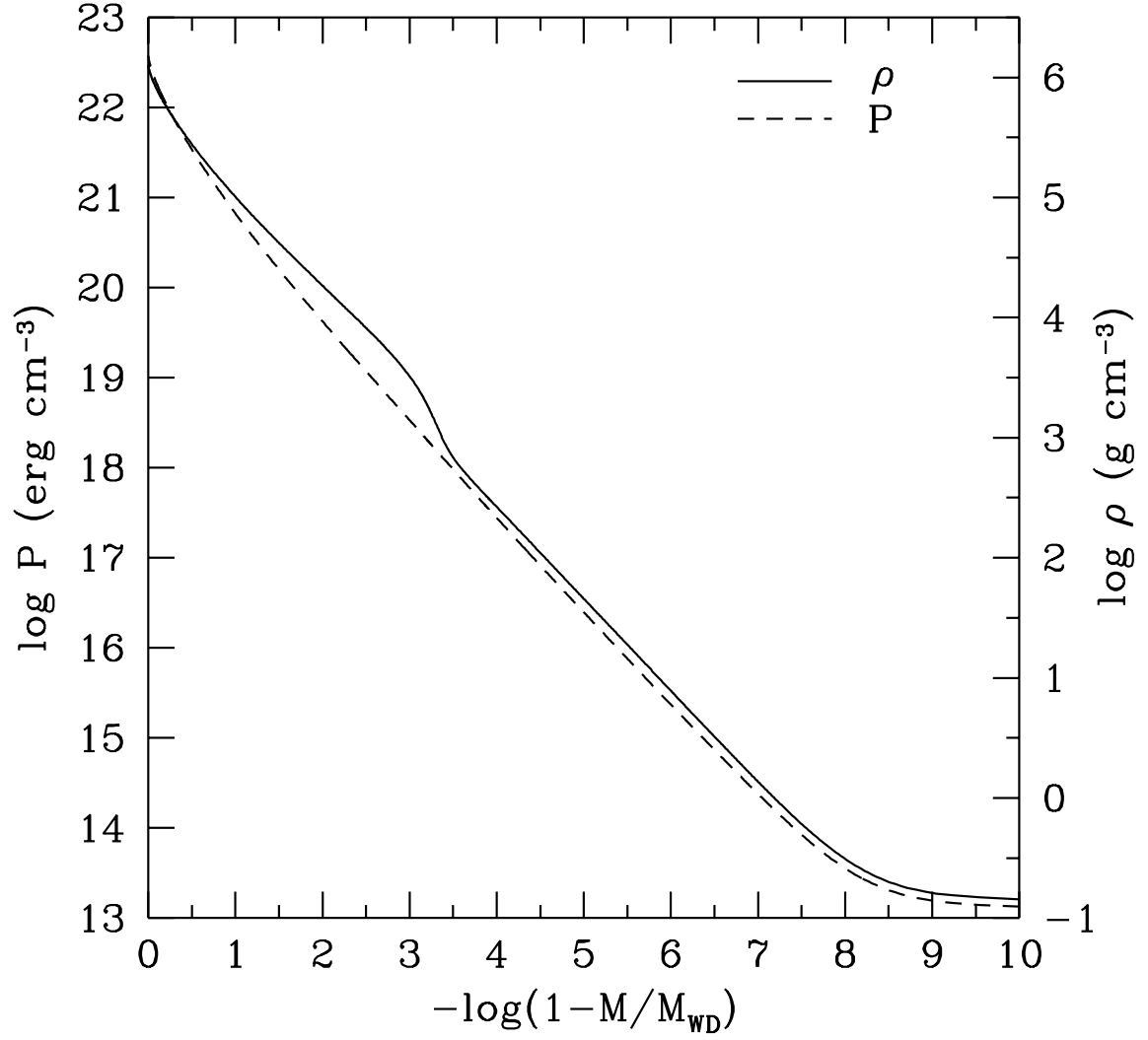


Fig. 1.— Pressure and density profiles of a  $0.43 M_{\odot}$  He WD, as a function of the mass coordinate  $\log(1 - M_r/M_{\text{WD}})$ . This coordinate allows to better resolve the very outer layers of the star, where the effects of the shock are presumably more important. The central temperature of the WD is  $10^7$  K.

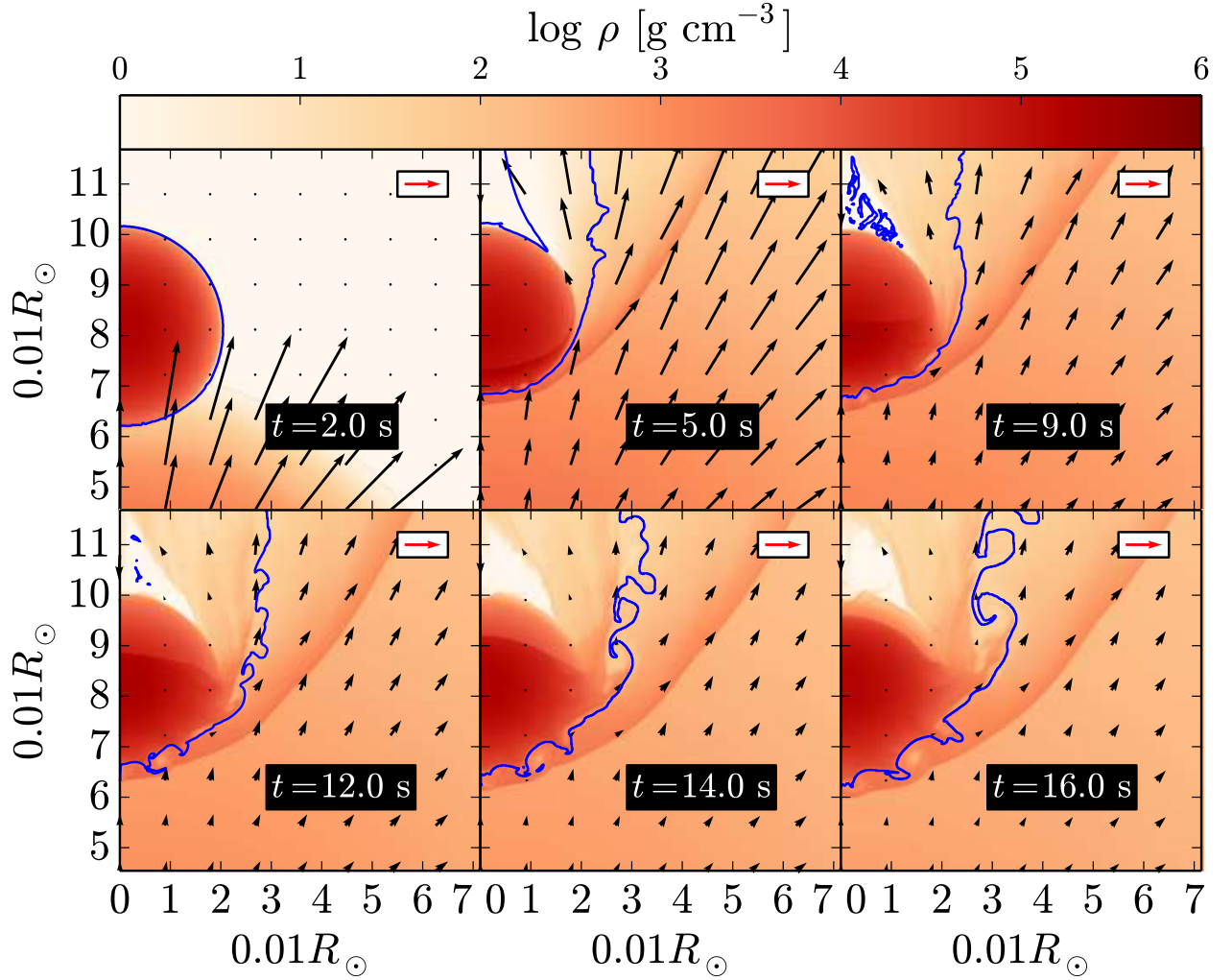


Fig. 2.— Density maps in the meridional plane at 6 times for the case in which a  $0.2M_{\odot}$  WD is adopted. The time elapsed since explosion is indicated in each panel. The simulation starts 2 s after explosion. The symmetry axis is along the left edge, and the origin of the grid (outside the plots) is at the center of the exploding CO WD. The blue line encloses the volume where the local helium mass fraction is  $Y > 0.5$ ; this represents the He WD and the material removed from the He WD. Prominent features include a shock running around the WD, and the formation of a dense conical surface in the expanding ejecta. The shock just reaches the back edge of the He WD at  $t = 16$  s. Temperatures and densities are too low to drive any significant nuclear burning. The plots are from the high-resolution run. The lower resolution simulation results in a similar structure. Velocity is proportional to the arrow length, with the inset showing an arrow for  $10,000 \text{ km s}^{-1}$ . Note the very fast gas at the outskirts, having velocities larger than the initial speed of  $20,000 \text{ km s}^{-1}$ . This very low mass gas was accelerated by the initial thermal energy that was non-negligible. When the ejecta is inserted with low temperatures no such velocities are achieved; the differences from the present run are very small (see version V1 on astro-ph).

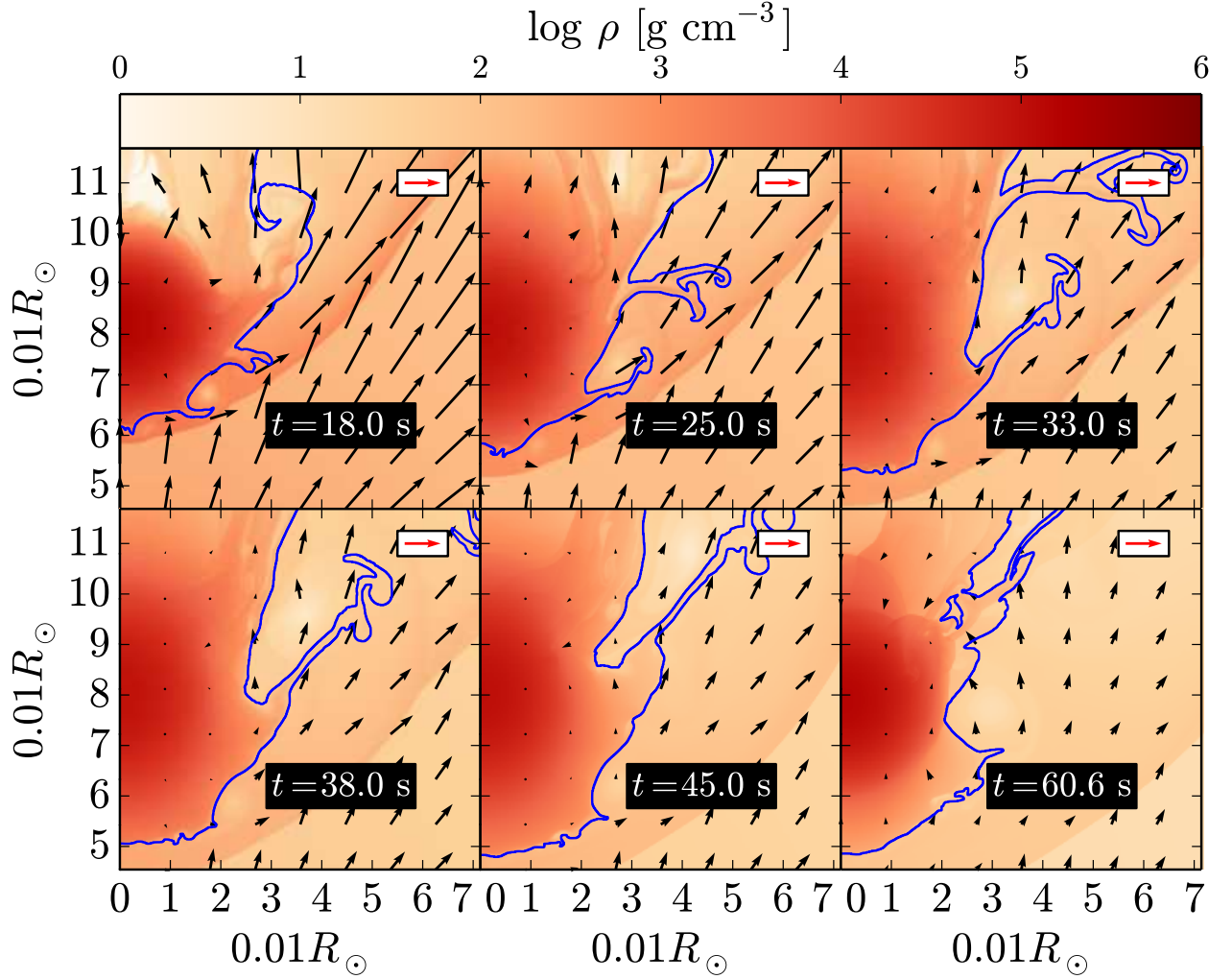


Fig. 3.— Same as Fig. 2 for later times, the intermediate stage. The shock breaks out from the rear of the WD, ejecting helium. Only  $0.003M_{\odot}$  of helium escapes while most of the helium falls back on the WD as can be seen in the last panel. The plots are from the low-resolution run. Velocity is proportional to the arrow length, with the inset showing an arrow for  $10,000 \text{ km s}^{-1}$ .

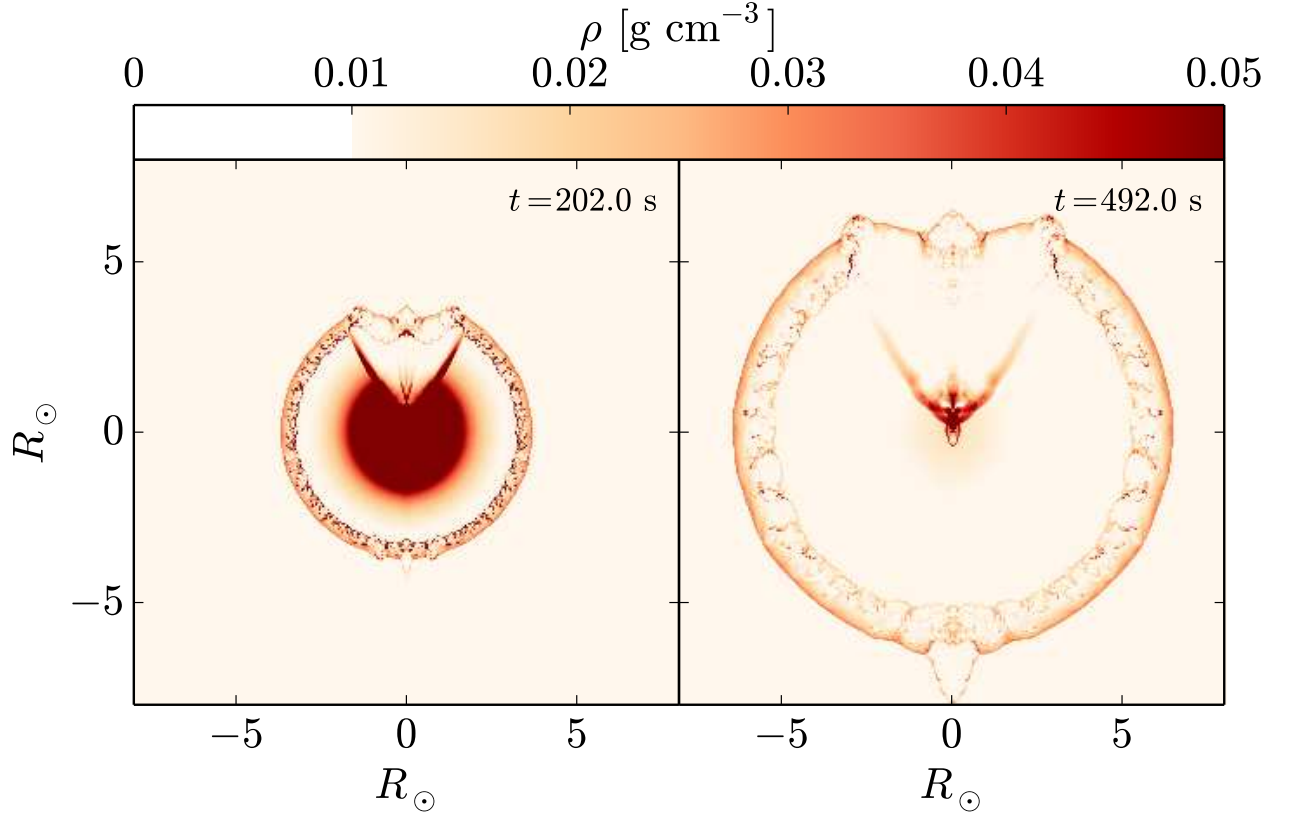


Fig. 4.— Density maps in the meridional plane at 2 late times for the case in which a  $0.2M_{\odot}$  WD is adopted. The computational grid was folded around the axis to present the entire meridional plane. A homologous expansion of the ejecta, with a Mach number  $> 10$ , has developed by the beginning of this evolutionary phase, with a dense conical surface surrounding a conical volume almost completely devoid of SN ejecta. The ambient gas density is fixed by our requirement that at the end of the simulation the ejecta sweeps a substantial mass (see text). At the end of our simulations,  $t = 492$  s, the SN ejecta has swept  $1M_{\odot}$  of ambient gas. As the outflow of the ejecta is already homologous, the morphology obtained here mimics that at hundreds of years later. The small features along the symmetry axis itself, both at the top and bottom of the SN-ISM interaction, are numerical artifacts.

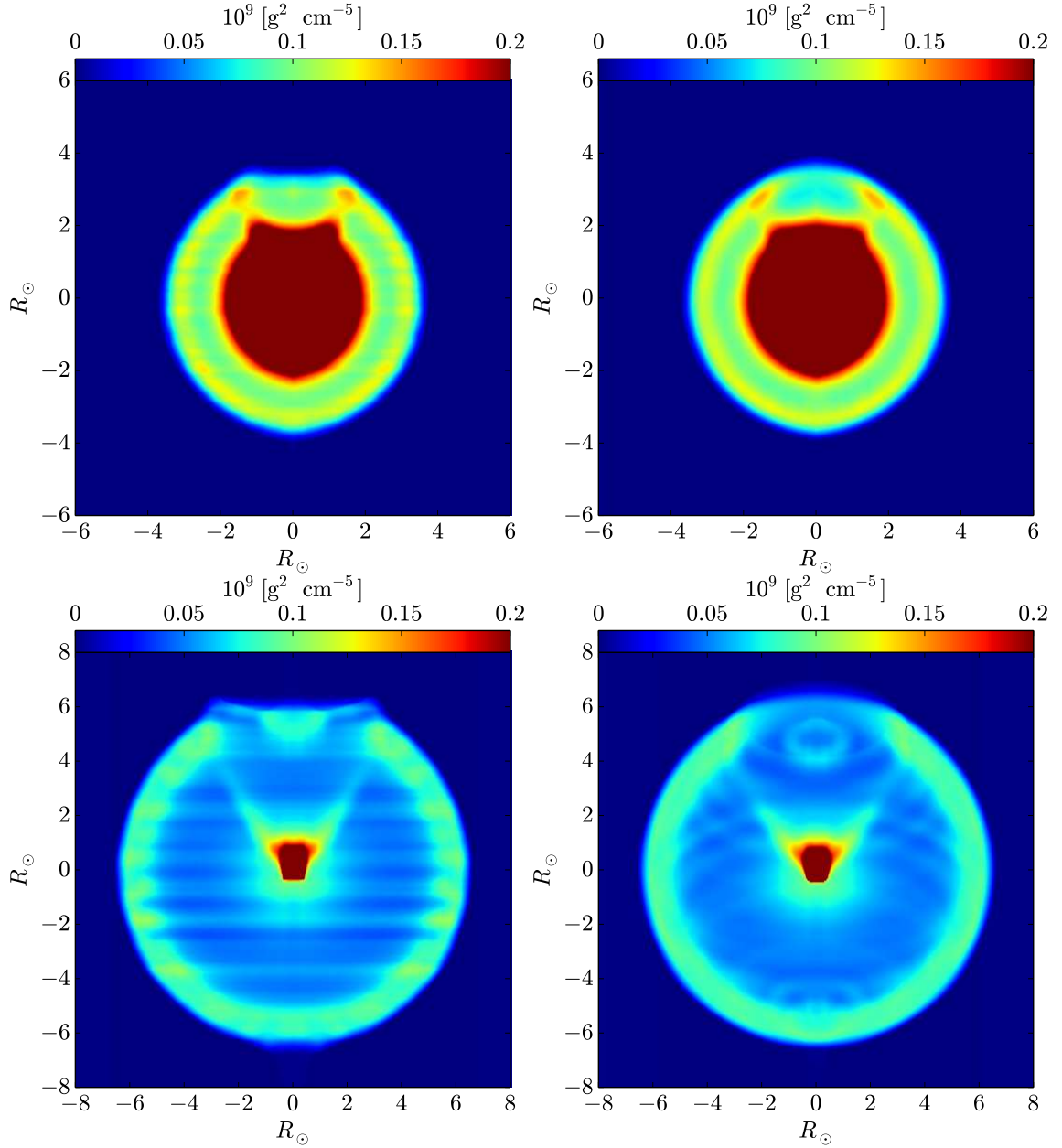


Fig. 5.— Synthetic observed morphology (eq. 8) of the resulting SNR for the case of a low-mass He WD. We show the intensity map described in the main text, and only for the high-temperature gas. The  $x$  and  $y$  coordinates are on the plane of the sky, and the  $z$  coordinate is taken along line of sight. Two inclinations are presented, the symmetry axis is in the plane of the sky (left), or at  $30^\circ$  to the plane of the sky (right). These are presented at two times, namely when the swept-up ambient masses are  $\sim 0.1M_\odot$  ( $t = 202$  s upper panels), and  $\sim 1M_\odot$  ( $t = 492$  s lower panels). As the outflow of the ejecta is already homologous at the beginning of this phase, the morphologies obtained here mimic that at hundreds of years later when the ejecta interacted with  $\sim 0.1 - 1M_\odot$  of homogeneous ambient medium (CSM or ISM).

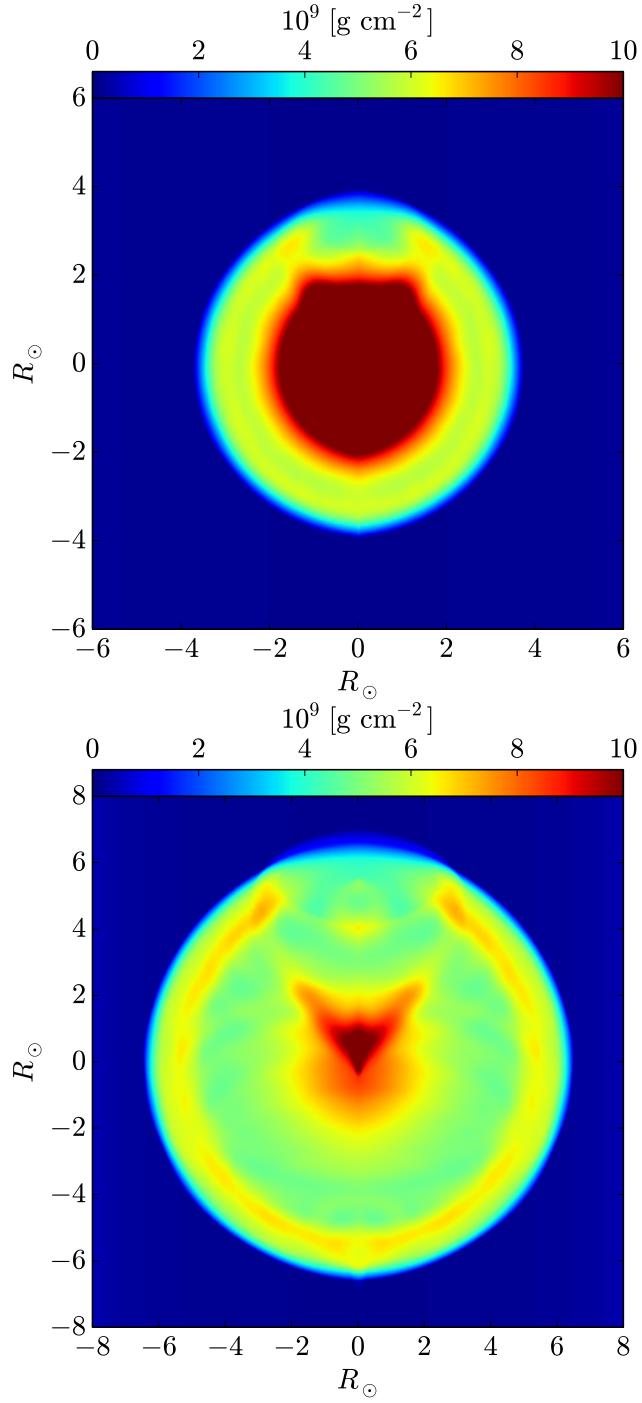


Fig. 6.— The integrated ejected mass (eq. 9) for the two times as in Fig. 5, and for the symmetry axis at  $30^\circ$  to the plane of the sky. Note the very low fraction of ejecta in the shadow behind the He WD (upper part in the figures) close to the edge of the remnant.



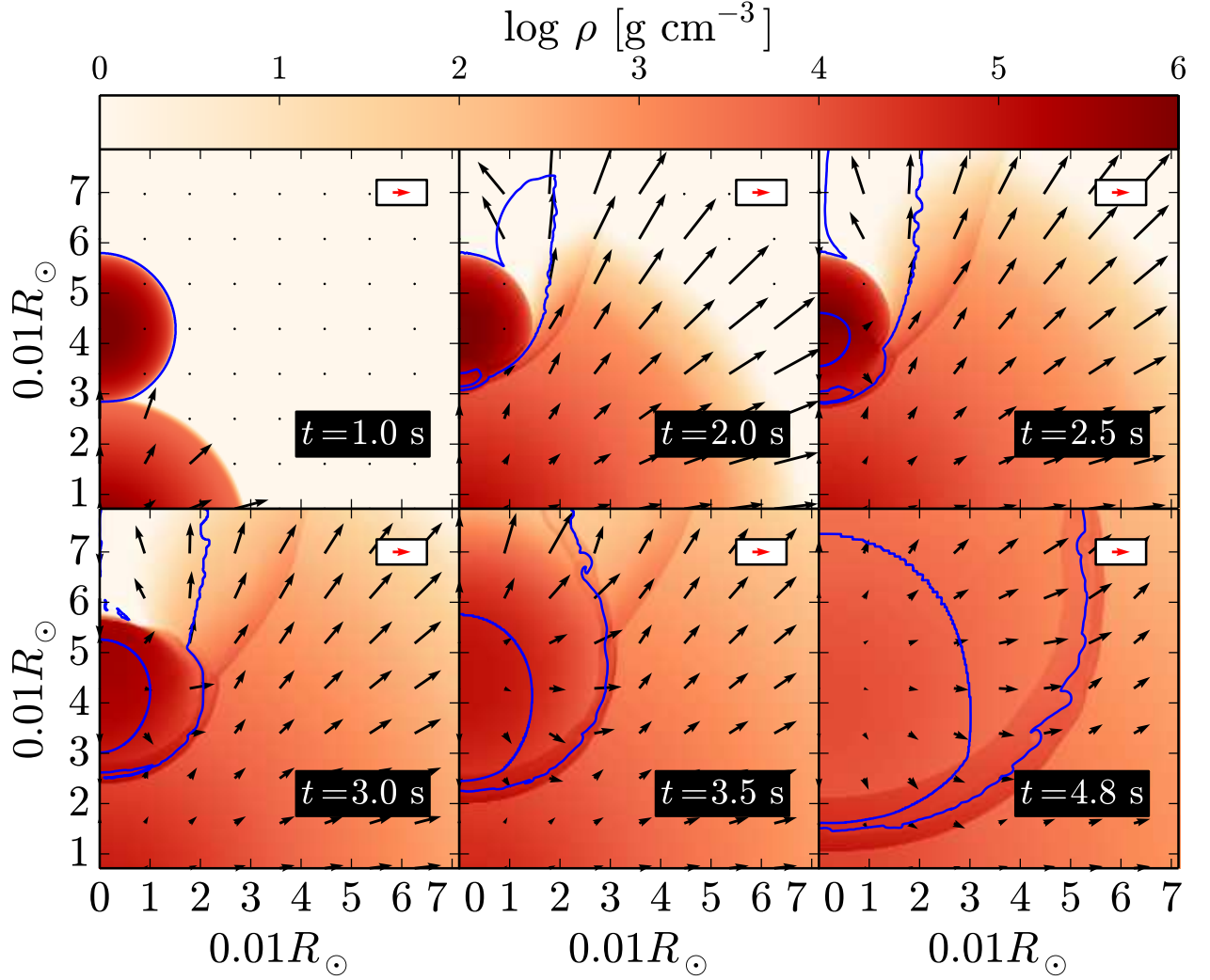


Fig. 7.— Density maps in the meridional plane at six times for a He WD of  $0.43M_{\odot}$  at an initial distance of its center to the center of explosion of  $0.045R_{\odot}$ . Note that at  $t = 2$  s helium is ignited and an explosion occurs in the He WD. The velocities are proportional to the arrow length, with the inset showing an arrow for  $10,000 \text{ km s}^{-1}$ .

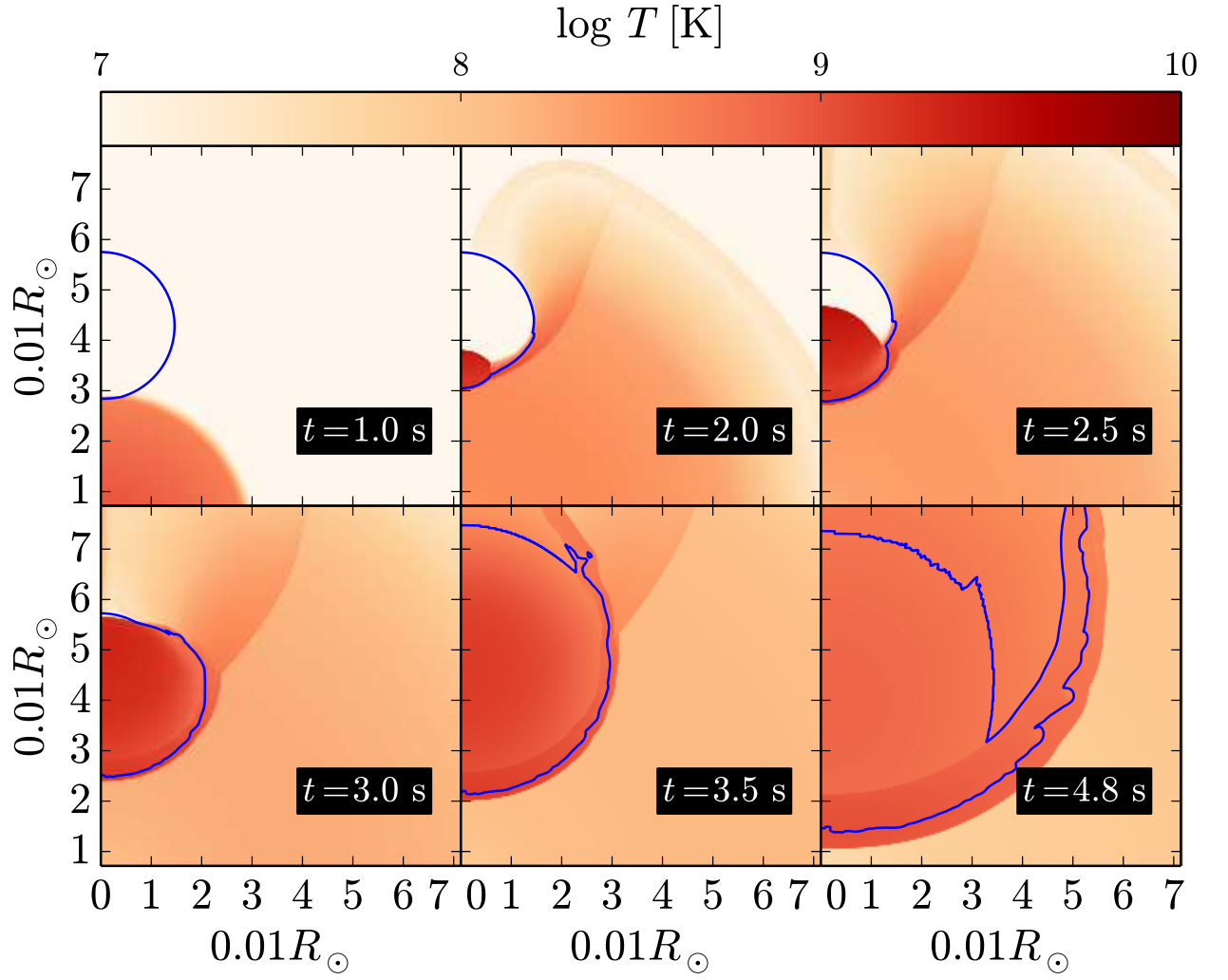


Fig. 8.— Same as Fig. 7 but for temperature.

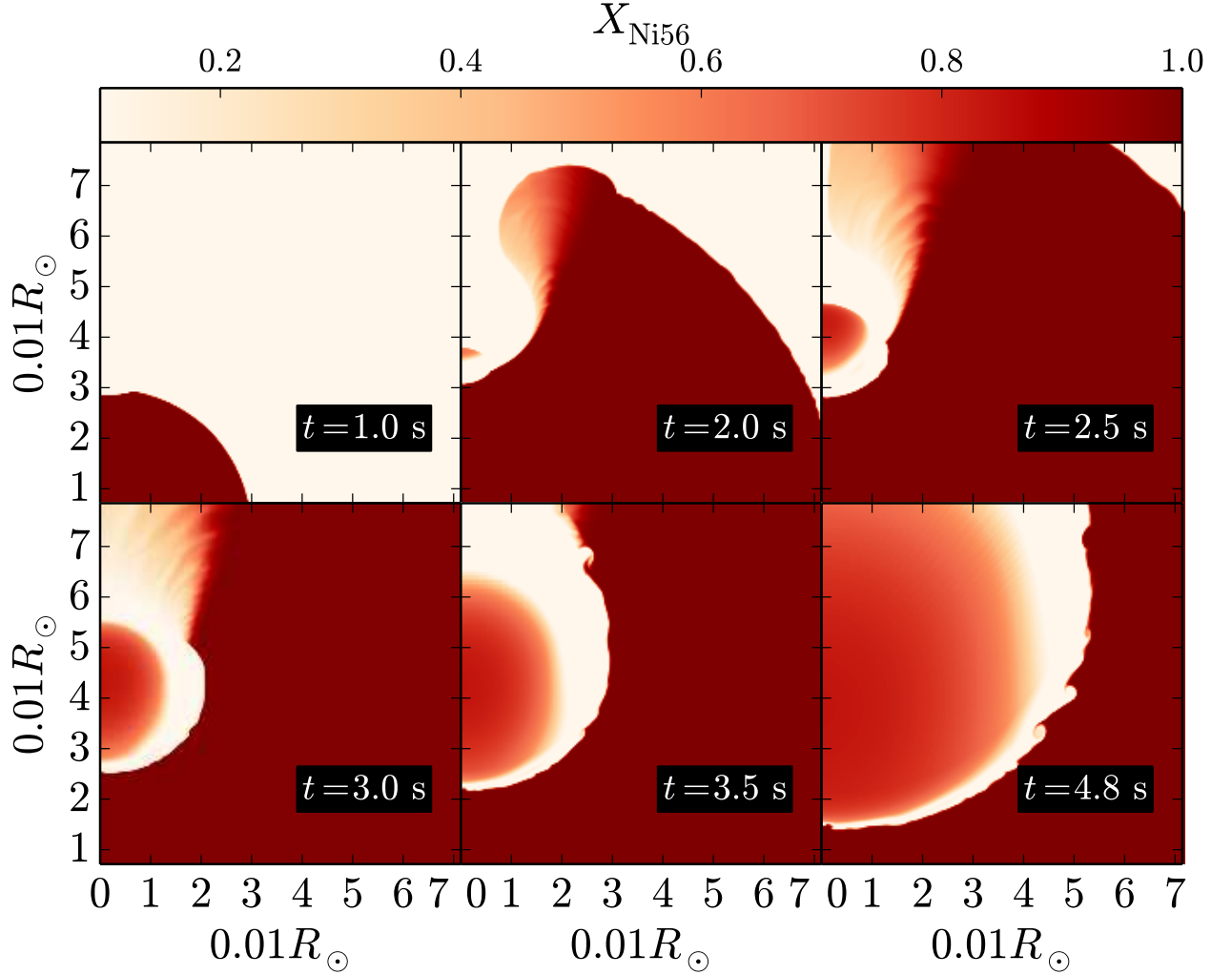


Fig. 9.— Same as Fig. 7 but for the nickel mass fraction. Ignition of helium in the He WD occurs just before  $t = 2$  s. The deep-red indicates the ejecta gas, that we took to be composed entirely of nickel. (Using CO composition for the ejecta does not change the results; see version V1 of the paper on astro-ph.). The lighter-red is the nickel mass fraction that is synthesized in the He WD. White regions are composed of He WD gas that did not form nickel.

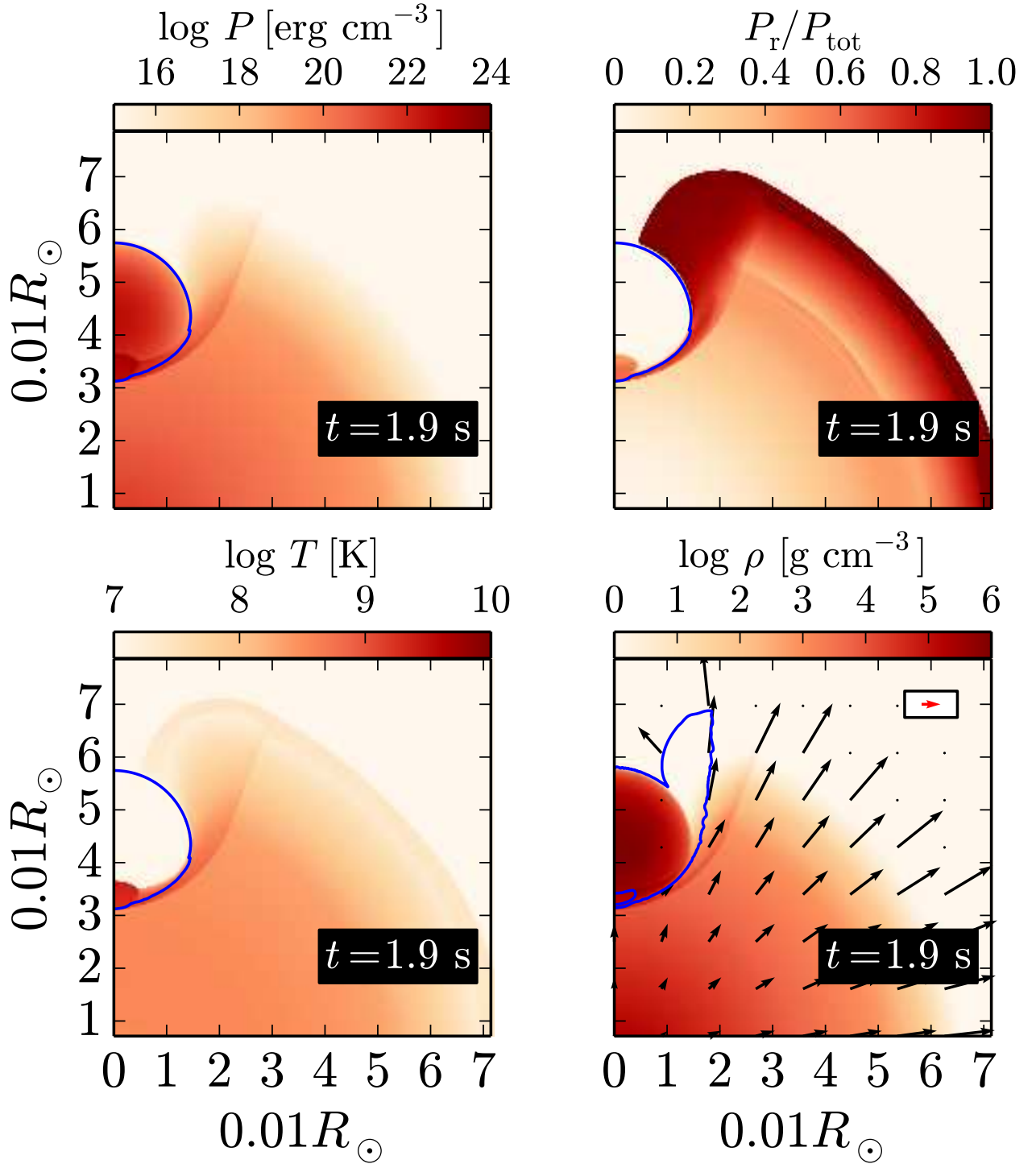


Fig. 10.— Total pressure (top left), ratio of radiation to total pressure (top right), temperature (bottom left), and density (bottom right) at  $t = 1.8$  s, just after He ignition. The velocities are proportional to the arrow length, with the inset showing an arrow for  $10,000$  km s $^{-1}$ . The blue line shows when the helium fraction is  $Y = 0.5$ . The figure is for the case in which a He WD of mass  $0.43M_{\odot}$  is adopted.